AIAA JOURNAL
Vol. 34, No. 4, April 1996

Dynamic Effects of Piezoactuators on the Cylindrical Shell Response

Venkata R. Sonti*
Automated Analysis Corporation, Peoria, Illinois 61602
and
James D. Jones†
Purdue University, West Lafayette, Indiana 47907

Dynamic effects of the mass and stiffness of a piezoactuator ring surface-bonded to a cylindrical shell are investigated. Wave propagation techniques are used. A curved actuator model (which neglects actuator mass and stiffness) developed in a companion study is compared with the composite model (case) involving properties of the actuator also. The curved model in general compares well with the composite case for low off-resonance frequencies where the modal densities are low. The model predicts the response well even up to half the shell thickness. At resonances, the dynamic effects of the actuator are significant, and since the model neglects these effects, the comparison is poor. However, for small thickness the model predicts reasonably well. At high frequencies where the modal densities are high, the response of the model differs significantly from the composite case. It is seen that at resonances the mass effect seems to dominate at higher thickness of the actuator. Because of this, there is evidence that the model will do better for smaller size of actuators.

Introduction

PIEZOACTUATORS in application to active structural acoustic control (ASAC) have generated a significant interest in the recent past.[1–9] They offer several advantages over the conventional point actuators, including their low weight, low cost, space efficiency, and others. Studies have shown that bimorph configured in-phase driven actuators have potential for reducing control spillover in ASAC of cylindrical shells.[6,7]

In a companion paper,[10] an analytical model for a curved bimorph in-phase driven actuator pair was derived in which approximate expressions for the equivalent forces exerted on the cylindrical shell were determined. Several simplifying assumptions were made. The actuators and the shell were assumed perfectly bonded, which resulted in the absence of interfacial shear stress and the continuity of normal strain across the interface. It was assumed that the Poisson's ratios of the actuator and the shell material were equal. Also, the Young's moduli, the thicknesses, and the Poisson's ratios of the layers involved were assumed constant within the actuator patch boundary. The composite was assumed thin in relation to the shell radius, thus making Love's thin-shell theory applicable. From the composite element in static equilibrium, an estimate of the equivalent forces exerted by the piezoactuator on the shell was obtained. These equivalent force expressions were directly incorporated in the dynamic shell equations. This implies that the shell behaves in a manner as if a force was exerted without the dynamics (stiffness and mass effect) of the actuator. Static stiffness of the actuator was accounted for by estimating the magnitude of the force resisted separately by the actuators and the shell. It is evident that several of these small piezoactuator patches will be required to achieve ASAC of a large cylindrical shell. Thus, the static and dynamic effects of the multiple actuators will no longer be negligible and will affect the system response by changing the natural frequencies of the original shell. In this investigation, an estimate of the dynamic effect of the actuator stiffness and mass is presented. Also, the actuator thickness range, the excitation frequency range, and the shell modes for which these models give accurate results for a particular size shell are determined, thus verifying the accuracy of the static curved model derived in the companion paper.[10]

The response of a system consisting of a simply supported finite cylindrical shell with a piezoelectric actuator ring bonded (inside and outside) all around the circumference at the centerline of the shell is considered (Fig. 1). The x direction line force and the transverse pressure force are considered separately. Response due to θ direction in-plane line force is not possible using this configuration, but the behavior may be deduced from the equivalent forces considered. Also, the responses are computed separately for each circumferential mode order, i.e., the equivalent force has a $\cos(n\theta)$ profile around the shell circumference. A wave approach is used in obtaining the response. The wave approach makes it easier to study the effects of actuator stiffness and mass simultaneously and separately. Also the curved model developed in Ref. 10 can be used with the wave approach in obtaining the response that gives a comparison between accounting for the actuator effects and neglecting them. In the composite portion of the cylinder/actuator system, an equivalent modulus approach is employed. This is valid because, first, it is assumed that the combined shell and actuator system are thin and Love's shell theory is applicable, and second, the structural wavelengths at the frequencies of interest are much larger than the combined shell and actuator thickness.

Since the approach involves the propagation of waves, a brief introduction to wave behavior in cylindrical shells is presented in the following section before dealing with the details of the shell response.

Waves in Cylindrical Shells

The composite equations of motion for a cylindrical shell bonded

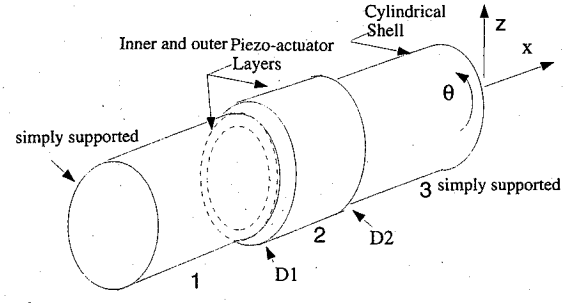

Fig. 1 Cylindrical shell with inside and outside surface-bonded ring piezoactuators.

Received Sept. 14, 1994; revision received May 17, 1995; accepted for publication May 17, 1995.

*Senior Project Engineer, 6516 N. University, Apartment 704.
†Professor, School of Mechanical Engineering, 1077 Ray W. Herrick Laboratories.

with piezoactuators on the inner and the outer surface are given by[10,14]

$$\left(\frac{Y_s}{1-\mu^2}h_1+2\frac{Y_{pe}}{1-\mu^2}h_2\right)\left[\frac{\partial}{\partial x}(S_{xx}+\mu S_{\theta\theta})+\frac{1+\mu}{2a}\frac{\partial}{\partial\theta}S_{x\theta}\right]-\rho h\ddot{u}_x=2\frac{Y_{pe}}{1-\mu^2}h_2\frac{\partial}{\partial x}\left(\Delta_x^0+\mu\Delta_\theta^0\right) \quad (1)$$

$$\left(\frac{Y_s}{1-\mu^2}h_1+2\frac{Y_{pe}}{1-\mu^2}h_2\right)\times\left[\frac{1}{a}\frac{\partial}{\partial\theta}(S_{\theta\theta}+\mu S_{xx})+\left(\frac{1-\mu}{2}\right)\frac{\partial}{\partial x}S_{x\theta}\right]+\left[\frac{Y_s}{1-\mu^2}\left(\frac{\delta_{t1}^3-\delta_{b1}^3}{3}\right)+2\frac{Y_{pe}}{1-\mu^2}\left(\frac{\delta_{t2}^3-\delta_{b2}^3}{3}\right)\right]\times\left[\frac{1}{a^2}\frac{\partial}{\partial\theta}(K_{\theta\theta}+\mu K_{xx})+\frac{1+\mu}{2a}\frac{\partial}{\partial x}K_{x\theta}\right]-\rho h\ddot{u}_\theta=2\frac{1}{a}\frac{Y_{pe}}{1-\mu^2}h_2\frac{\partial}{\partial\theta}\left(\Delta_\theta^0+\mu\Delta_x^0\right) \quad (2)$$

$$\left[\frac{Y_s}{1-\mu^2}\left(\frac{\delta_{t1}^3-\delta_{b1}^3}{3}\right)+2\frac{Y_{pe}}{1-\mu^2}\left(\frac{\delta_{t2}^3-\delta_{b2}^3}{3}\right)\right]\times\left[\frac{\partial^2}{\partial x^2}(K_{xx}+\mu K_{\theta\theta})+\frac{2}{a}\left(\frac{1-\mu}{2}\right)\frac{\partial^2}{\partial x\partial\theta}K_{x\theta}+\frac{1}{a^2}\frac{\partial^2}{\partial\theta^2}(K_{\theta\theta}+\mu K_{xx})\right]-\frac{1}{a}\left(\frac{Y_s}{1-\mu^2}h_1+2\frac{Y_{pe}}{1-\mu^2}h_2\right)\times(S_{\theta\theta}+\mu S_{xx})-\rho h\ddot{u}_z=-2\frac{1}{a}\frac{Y_{pe}}{1-\mu^2}h_2\left(\Delta_\theta^0+\mu\Delta_x^0\right) \quad (3)$$

where Y_{pe} and Y_s are the Young's moduli of the piezoactuator and the shell, respectively, μ is the assumed Poisson's ratio (same for both shell and piezoactuator), and a is the radius of the shell. The variables S_{xx}, $S_{\theta\theta}$, and $S_{x\theta}$ are the membrane strain vector components, whereas K_{xx}, $K_{\theta\theta}$, and $K_{x\theta}$ are the bending strain vector components.[11] The variable h_1 is the thickness of the cylindrical shell, and h_2 is the thickness of the actuators (both actuators have the same thickness). The variable ρh stands for the summation of the product of the density and thickness for each of the layers in the composite. It is explicitly written as $\sum_i \rho_i h_i$, where the index $i = 1$ for the shell and $i = 2, 3$ for the piezoactuators. The variables Δ_x^0 and Δ_θ^0 represent the free strain components of the piezoactuator in the axial and the circumferential directions, respectively. The variables δ_{t1} and δ_{b1} represent the distances of the top and the bottom layers of the shell from the neutral axis of the composite. These distances are given by δ_{t2} and δ_{b2} for the piezoactuators. For the actuator on the inner surface they have negative values. The axial, torsional, and transverse displacements are given by u_x, u_θ, and u_z, respectively. Details of the preceding equations are given in a companion paper[10] and in Ref. 14. In the preceding equations the piezoactuator terms may be dropped if homogenous shell equations are required. Since the inherent composite shell wave behavior is investigated, for the time being, the right-hand side piezoelectric forcing terms are ignored.

The relation between frequency and wave number (commonly known as the dispersion relation) for the composite shell is found assuming the following solution[12]:

$$u_x=\sum_{s=1}^{4}\sum_{n=0}^{\infty}U_{xns}\cos(n\theta)\exp(-jk_{ns}x+j\omega t+j\pi/2) \quad (4)$$

$$u_\theta=\sum_{s=1}^{4}\sum_{n=0}^{\infty}U_{\theta ns}\sin(n\theta)\exp(-jk_{ns}x+j\omega t) \quad (5)$$

$$u_z=\sum_{s=1}^{4}\sum_{n=0}^{\infty}U_{zns}\cos(n\theta)\exp(-jk_{ns}x+j\omega t) \quad (6)$$

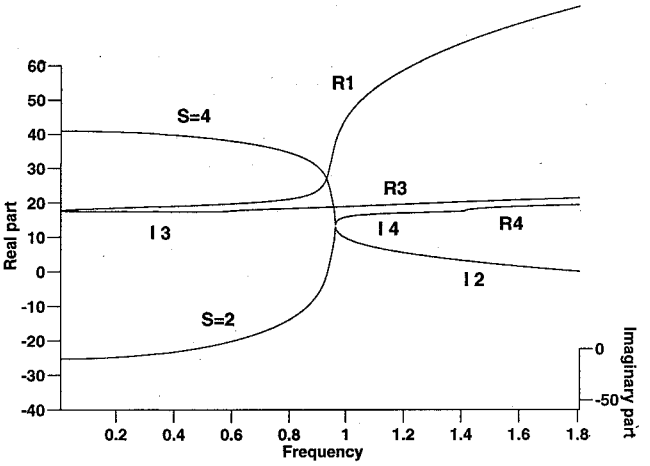

Fig. 2 Waves in a homogenous cylindrical shell (two-dimensional view): a = 0.75 m and *h*1 = 0.002 m.

where the variable n refers to the circumferential mode number, and k_{ns} refers to the wave number where s is the wave type (transverse, nearfield, torsion, and axial) associated with a particular wave number. The variables U_{xns}, $U_{\theta ns}$, and U_{zns} are the axial, torsional, and transverse displacements related to the specific wave numbers k_{ns}. Substitution of these solutions in the equations of motion (1–3) results in the dispersion relations that may be written in a matrix notation as

$$[D]\begin{bmatrix}U_{xns}\\U_{\theta ns}\\U_{zns}\end{bmatrix}=0 \quad (7)$$

The expression for D using Love's shell theory is given in Ref. 13. The roots of the determinant of D are the required wave numbers. For a cylindrical shell the determinant is eighth order, and so eight values for the wave number are obtained. Thus, four waves propagate in the positive x and four in the negative x direction. These waves include a propagating wave primarily in the transverse direction ($s = 1$), a transverse near-field effect ($s = 2$), a propagating wave primarily torsional ($s = 3$), and the last propagating and primarily axial ($s = 4$) (see Fig. 2). Each of the four waves has a maximum amplitude in one direction (known as the primary direction) and also components in the other two coordinate directions. This is due to coupling resulting from the shell curvature. Once the wave number is computed, the fraction of motion in the other two directions may be obtained by substituting the wave number in the dispersion relation. Absolute magnitudes are obtained only after the amplitude is obtained in the primary direction. For the present, only the ratios are known. For example, wave 4 (k_{n4}) is primarily axial, and thus its fractional components in the transverse and circumferential directions (U_{zn4}/U_{xn4} and $U_{\theta n4}/U_{xn4}$) may be obtained by substituting the value of the wave number in the dispersion equation. Any two of the three equations may be used.

The frequency dependence of the wave numbers is shown in Fig. 2 for a cylindrical shell of homogeneous material of radius a 0.75 m and thickness h 0.002 m. The numbers next to the curve denote the particular wave. The symbol R refers to purely real or propagating waves, I to purely imaginary or near-field effects, and S to complex waves. A small amount of damping is assumed in the shell material to simulate a more realistic system and is incorporated into the equations using a complex Young's modulus. The low-frequency behavior is quite different from that of the high frequency. This is because of the significant coupling caused by the curvature at low frequencies. The frequency behavior at high frequencies is similar to that of a flat plate (waves 1 and 2), a torsional (wave 3), and a longitudinal rod (wave 4). The frequency axis is normalized with respect to the extensional wave speed in the material. At the frequency value equal to 1 (known as the ring frequency), it may be seen that the torsional wave has already cut on and the transverse wave number rises sharply (see Fig. 2). In acoustic radiation of cylinders the ring frequency is of significance because typically

transverse modes that cut on below the ring frequency radiate sound efficiently. This is because the structural wave number is smaller than the acoustic wave number, thus making the wavelength longer. This is quite unlike flat plates where below coincidence (a condition where the acoustic wave number equals to the structural wave number) the acoustic wave number is smaller than the structural wave number. This phenomenon in cylinders is again due to the curvature that couples the membrane and flexural behavior.

Shell Response Due to Various Piezoactuator Equivalent Forces

In this section, the mathematical details of obtaining the response of a finite simply supported cylindrical shell bonded with two rings of piezoactuators (one inside and one outside) are presented (Fig. 1).

As explained in the previous section, the wave number k_{ns} is dependent on the shell material constants, the radius, the thickness, and the frequency. The roots of the determinant in Eq. (7) give the wave number values. Thus, the unknowns in Eqs. (4–6) are amplitudes of the various waves U_{xns}, $U_{\theta ns}$, and U_{zns}. The shell actuator system is divided into three regions (Fig. 1). Regions 1 and 3 represent the homogenous shell region, and 2 is the composite region with the piezoactuators. Since eight waves are present in each of the sections, there are 24 wave amplitudes to be solved for. These are solved using boundary conditions and continuity conditions. For a simply supported cylindrical shell, four boundary conditions are required at each end for uniqueness. These conditions are

$$\begin{aligned} u_\theta &= 0 \\ u_z &= 0 \\ N_{xx} &= 0 \\ M_{xx} &= 0 \end{aligned} \tag{8}$$

where u_θ and u_z are the tangential and transverse displacements, and N_{xx} and M_{xx} are the axial force and axial moment resultants, respectively. At the first (between regions 1 and 2) and second (between regions 2 and 3) interfaces (shown as D1 and D2), eight continuity equations are required. These include the continuity of u_x, u_θ, u_z, $\partial u_z/\partial x$, N_{xx}, $N_{x\theta}$, Q_{xz}, and M_{xx}. The expressions for each of the variables are given in Ref. 11. Thus, we have 24 unknowns and 24 equations that can be easily solved. To include the dynamic mass and stiffness effect of the piezoactuators the wave numbers k_{ns} are solved using the composite equations (1–3). To include either the stiffness or the mass, the wave numbers are obtained by setting the appropriate variable (density or Young's modulus) in Eqs. (1–3) to zero. Similarly, the homogenous shell wave numbers are obtained by setting both the density and Young's modulus of the actuator to zero. The final set of equations have the form

$$Ay = B \tag{9}$$

where A is a 24×24 matrix, y is the vector of the 24 wave amplitudes, and B is the vector involving external forces. Methods to include the forcing are discussed separately as each equivalent force model is evaluated in the following sections.

In the following sections the response of a simply supported cylindrical shell bonded with two rings of piezoactuators (one on the inside and one on the outside) is presented (Fig. 1). The axial centerline of the actuators coincides with that of the shell. The cylinder has a length L of 3.0 m, a radius a of 0.75 m, and thickness h equal to 0.002 m. The shell material (steel) has a Young's modulus of $2.07e11$ N/m^2 and a density of 7850.0 kg/m^3. The piezoceramic actuator has a Young's modulus of $0.67e11$ N/m^2 and a density of 7000.0 kg/m^3. Both the materials are assumed to have a Poisson's ratio of 0.31 due to reasons discussed in Refs. 10 and 14. The x-direction line force and the transverse pressure are considered. Various cases are studied to estimate the dynamic effect of the actuator stiffness and mass. The response to a θ in-plane line force may be deduced from the results due to the equivalent forces considered. Because of limitations on the length of the manuscript, only a few of the cases studied are presented.

The curved thin bimorph configured in-phase driven piezoactuators surface bonded to a cylindrical shell exert the following equivalent forces:

$$\begin{aligned} F_x &= 2\frac{\left[Y_s/(1-\mu^2)\right]h_1}{\left\{\left[Y_s/(1-\mu^2)\right]h_1 + 2\left[Y_{pe}/(1-\mu^2)\right]h_2\right\}} \\ &\quad\times \frac{Y_{pe}}{1-\mu^2}h_2\frac{\partial}{\partial x}\left(\Delta_x^0 + \mu\Delta_\theta^0\right) \\ F_\theta &= 2\frac{\left[Y_s/(1-\mu^2)\right]h_1}{\left\{\left[Y_s/(1-\mu^2)\right]h_1 + 2\left[Y_{pe}/(1-\mu^2)\right]h_2\right\}} \\ &\quad\times \frac{1}{a}\frac{Y_{pe}}{1-\mu^2}h_2\frac{\partial}{\partial\theta}\left(\Delta_\theta^0 + \mu\Delta_x^0\right) \\ F_z &= 2\frac{\left[Y_s/(1-\mu^2)\right]h_1}{\left\{\left[Y_s/(1-\mu^2)\right]h_1 + 2\left[Y_{pe}/(1-\mu^2)\right]h_2\right\}} \\ &\quad\times \frac{1}{a}\frac{Y_{pe}}{1-\mu^2}h_2\left(\Delta_\theta^0 + \mu\Delta_x^0\right) \end{aligned} \tag{10}$$

where F_x is a line force in the in-plane x direction, F_θ is a line force in the in-plane θ direction, and F_z is the transverse z direction pressure load. For details see Refs. 10 and 14.

Shell Response to x Line Force

In presenting the response due to the x-direction line force (see Fig. 3) exerted by the piezoactuator, four different cases are investigated for every circumferential mode n and frequency combination. For the first case, the actuator model developed is used [i.e., the shell is homogenous with an applied force, Eq. (10) F_x], the second involves the full composite shell/actuator system [in computing the wave numbers the actuator stiffness and density are used, and the equivalent forces are the right side of Eq. (1)], the third case accounts only for the actuator stiffness (in computing the wave numbers for the composite region, the density is set to zero), and the fourth case involves only the density of the system (in computing the wave numbers for the composite part the stiffness is set to zero).

For the curved model case the x-direction line force expression is given by

$$\begin{aligned} F_{x1} &= 2\frac{\left[Y_s/(1-\mu^2)\right]h_1}{\left\{\left[Y_s/(1-\mu^2)\right]h_1 + 2\left[Y_{pe}/(1-\mu^2)\right]h_2\right\}} \\ &\quad\times \frac{Y_{pe}}{1-\mu^2}h_2\frac{\partial}{\partial x}\left(\Delta_x^0 + \mu\Delta_\theta^0\right) \end{aligned} \tag{11}$$

which is the expression from the curved model derived in Ref. 10. For the other three cases, the force expression is given by the right-hand side of Eq. (1), which includes both the shell and actuator properties, reproduced next for convenience,

$$F_x = 2\frac{Y_{pe}}{1-\mu^2}h_2\frac{\partial}{\partial x}\left(\Delta_x^0 + \mu\Delta_\theta^0\right) \tag{12}$$

The axial line force is exerted as shown in Fig. 3.

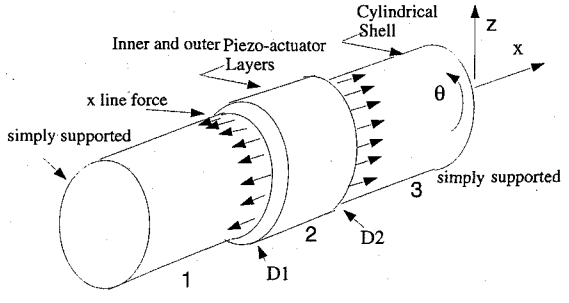

Fig. 3 Cylindrical shell with inside and outside surface-bonded ring piezoactuators, x line force.

Figures 4–8 show the response of the shell to the axial line force at a point ($x = 2.25, \theta = 0.0$) as a function of thickness ratio (actuator/shell thickness). The reason for choosing $x = 2.25$ is that for a 3-m-long shell it corresponds to a point away from the nodes of several odd axial order modes. The circumferential force profiles investigated include $n = 1, 2, 3, 4, 15$, and 16. But only resonances and off-resonances for $n = 3$ and 4 and an off-resonance for $n = 15$ are shown due to limitations on the length of the manuscript. Results of the other profiles are included in discussing the general trends. Each figure has four lines that, as mentioned earlier, are for the curved actuator model and the three cases with both actuator stiffness and density included, only stiffness included and only density included. For convenience in presentation, "model" will stand for the curved actuator model, the case including both the stiffness and density of the actuator will be known as the composite case or (plot), and the cases with either the actuator stiffness or mass will be known as the stiffness and the mass cases (plots), respectively. The frequencies and the resonant mode numbers are shown in the captions.

In general, at off-resonance frequencies the curved model compares well with the composite case at times even up to half the thickness of the shell (see Figs. 5 and 7). Typically, the composite response is less than the cases involving stiffness or the mass exclusively. This is because away from resonance both of these properties reduce the response and the combination of the two has an even stronger reducing effect. At resonance frequencies, the model

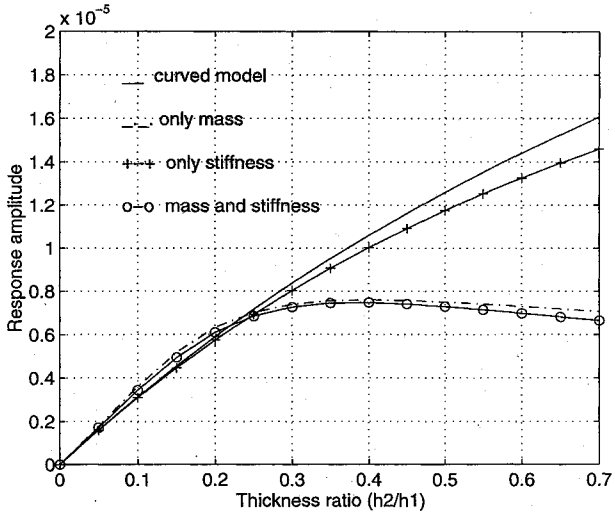

Fig. 4 Shell response as a function of thickness ratio; x line force and (3, 3) mode resonance frequency of 394 Hz.

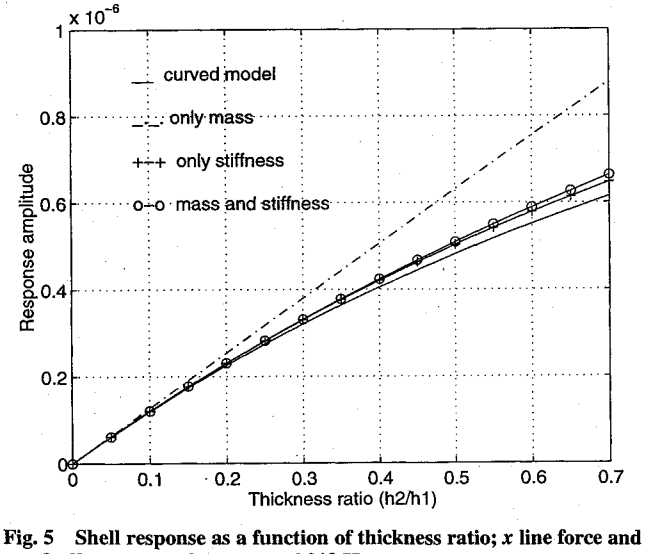

Fig. 5 Shell response as a function of thickness ratio; x line force and $n = 3$ off-resonance frequency of 318 Hz.

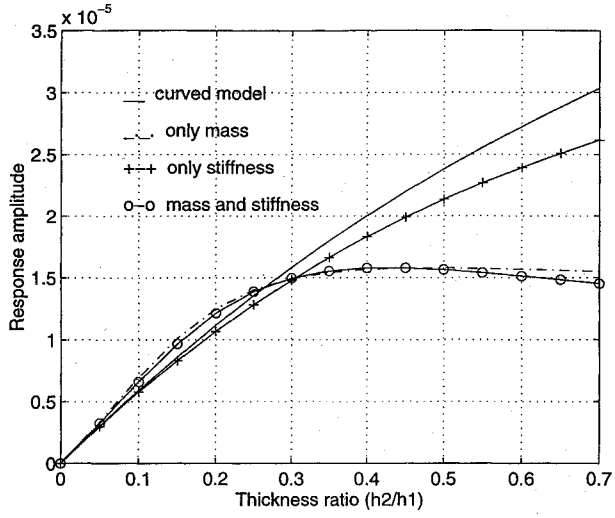

Fig. 6 Shell response as a function of thickness ratio; x line force and (3, 4) mode resonance frequency of 271 Hz.

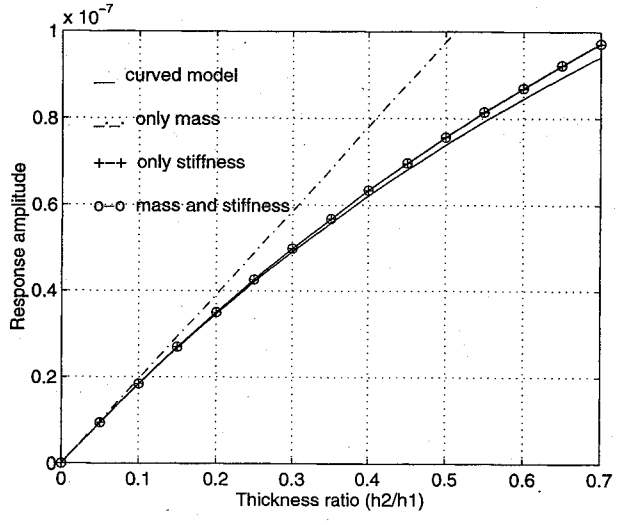

Fig. 7 Shell response as a function of thickness ratio; x line force and $n = 4$ off-resonance frequency of 398 Hz.

matches the composite case at most up to 0.5 mm, which is a fourth of the shell thickness (see Figs. 4 and 6). This trend is seen for $n = 1$ and 2 also. Beyond this thickness, the dynamic effects of the actuator dominate. The composite case and the mass case increase with thickness up to a point and then start going down beyond that point. The reason is that the axial line force increases with thickness and at low thicknesses the increasing force dominates, but beyond a point the increased mass of the actuator begins to reduce the response. Thus, it appears that the mass is the dominant effect near resonances. It is an indication that for smaller actuators the mass effect will not be so strong and the curved model will compare better with the composite case. Similarly, stiffness appears to be the dominant effect at off resonance frequencies since the composite plot tends to follow the stiffness case. At high frequencies where modal densities are high, several modes contribute even at off-resonances, and thus the model matches the composite case only up to one-fourth thickness ratio. At the higher order circumferential modes (Fig. 8, including the cases not shown), the four plots differ from each other considerably, and also the amplitudes of response are lower. This may be because the axial force does not couple so well into these higher order modes at high frequencies and the effects of different parameters (mass and stiffness of actuator) may be causing a stronger coupling between the force and shell. At this point it is unclear as to why the model performs so poorly for high circumferential orders. In active noise and vibration control (ANVC), the lower circumferential order shell modes radiate most of the noise,[6] and thus tailoring of piezoactuator dimensions, the location, and number to excite only the low n modes

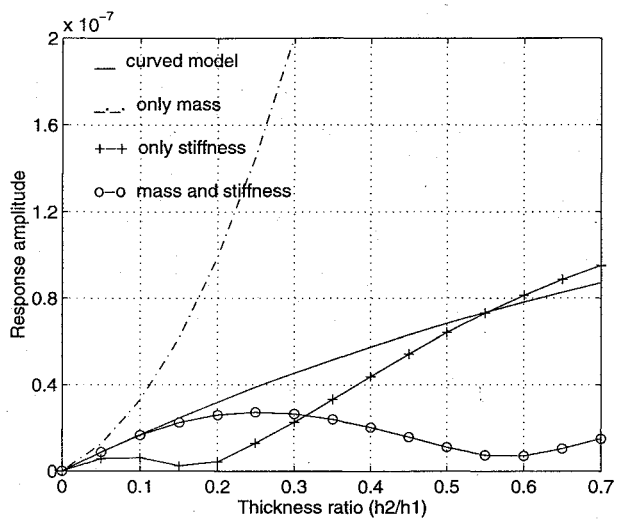

Fig. 8 Shell response as a function of thickness ratio; x line force and $n = 15$ off-resonance frequency of 1250 Hz.

is of significant interest. Under such conditions of excitation the current actuator model will perform well since responses at low n match the composite response.

Shell Response to Transverse Pressure

In this section, the response of the same cylindrical shell (with two rings of surface bonded actuators) to transverse pressure force is analyzed. The pressure has the variation of a particular circumferential mode in the θ direction (i.e., $n = 1, 2, \ldots$, etc.). As in the previous section, the pressure force model developed in Ref. 10 is compared with the "true" pressure force exerted when the actuator stiffness and mass effects are accounted for. Also, the responses of the shell with either the stiffness or the mass included are presented to understand the effects of these factors.

To include the pressure load, the following forcing function is chosen:

$$P_z \cos(n\theta) \tag{13}$$

where P_z is the constant pressure amplitude independent of x with a cosine profile in the θ direction. Thus, the shell equations are given by

$$\frac{\partial N_{xx}}{\partial x} + \frac{1}{a}\frac{\partial N_{x\theta}}{\partial \theta} - \rho_s h_s \frac{\partial^2 u_x}{\partial t^2} = 0 \tag{14}$$

$$\frac{\partial N_{x\theta}}{\partial x} + \frac{1}{a}\frac{\partial N_{\theta\theta}}{\partial \theta} + \frac{1}{a}\left(\frac{\partial M_{x\theta}}{\partial x} + \frac{1}{a}\frac{\partial M_{\theta\theta}}{\partial \theta}\right) - \rho_s h_s \frac{\partial^2 u_\theta}{\partial t^2} = 0 \tag{15}$$

$$\frac{\partial^2 M_{xx}}{\partial x^2} + \frac{2}{a}\frac{\partial^2 M_{x\theta}}{\partial x \partial \theta} + \frac{1}{a^2}\frac{\partial^2 M_{\theta\theta}}{\partial \theta^2} - \frac{N_{\theta\theta}}{a} - \rho_s h_s \frac{\partial^2 u_z}{\partial t^2} = P_z \cos(n\theta) \tag{16}$$

where $N_{x\theta}$ and $M_{x\theta}$ are the shear force and twisting moment resultants, and $N_{\theta\theta}$ and $M_{\theta\theta}$ are the force and the moment resultants in the θ direction, respectively. Also ρ_s is the density of the shell, h_s the thickness, and a the radius of the shell. In deriving these equations transverse shear strains and rotational inertia are neglected.

Since the forcing function is independent of x, the following particular solutions are assumed:

$$\begin{aligned} u_x &= U_{xmn} \cos(n\theta) \\ u_\theta &= U_{\theta mn} \sin(n\theta) \\ u_z &= U_{zmn} \cos(n\theta) \end{aligned} \tag{17}$$

and in the shell equations (14–16) the x-dependent terms are dropped. Substituting the stress and strain expressions from Ref. 10 for the stress and moment resultants, and dropping the x-dependent terms, the equations may be given by

$$\begin{aligned} &\left[-\frac{1}{2a^2}K_c(1-\mu)n^2 + \rho h\omega^2\right]U_{xmn} = 0 \\ &\left(-\frac{n^2}{a^2}K_c - \frac{n^2}{a^4}D_c + \rho h\omega^2\right)U_{\theta mn} \\ &\quad + \left(-\frac{n}{a^2}K_c - \frac{n^3}{a^4}D_c\right)U_{zmn} = 0 \\ &\left(-\frac{n^3}{a^4}D_c - \frac{n}{a^2}K_c\right)U_{\theta mn} \\ &\quad - \left(-\frac{n^4}{a^4}D_c - \frac{1}{a^2}K_c + \rho h\omega^2\right)U_{zmn} = P_z \end{aligned} \tag{18}$$

where the variables K_c and D_c represent the composite membrane and bending stiffness, respectively. The variable ρh is the sum of the products of density and thickness of all layers in the laminate. Three constants are defined as follows:

$$\begin{aligned} \alpha_1 &= \left(-\frac{D_c n^3}{a^4} - \frac{K_c n}{a^2}\right) \\ \alpha_2 &= \left(\rho h\omega^2 - \frac{D_c n^2}{a^4} - \frac{K_c n^2}{a^2}\right) \\ \alpha_3 &= \left(\rho h\omega^2 - \frac{D_c n^4}{a^4} - \frac{K_c}{a^2}\right) \end{aligned} \tag{19}$$

The solution thus is given by

$$\begin{aligned} U_{xmn} &= 0 \\ U_{\theta mn} &= \frac{P_z \alpha_1}{\alpha_2\alpha_3 - \alpha_1^2} \\ U_{zmn} &= \frac{P_z \alpha_2}{\alpha_2\alpha_3 - \alpha_1^2} \end{aligned} \tag{20}$$

The total solution is given by the sum of this particular solution and the homogenous solution given in Eqs. (4–6),

$$\begin{aligned} u_x &= \sum_{s=1}^{4}\sum_{n=0}^{\infty} U_{xns} \cos(n\theta) \\ &\quad \times \exp(-jk_{ns}x + j\omega t + j\pi/2) + U_{xmn}e^{j\omega t} \\ u_\theta &= \sum_{s=1}^{4}\sum_{n=0}^{\infty} U_{\theta ns} \sin(n\theta) \exp(-jk_{ns}x + j\omega t) + U_{\theta mn}e^{j\omega t} \\ u_z &= \sum_{s=1}^{4}\sum_{n=0}^{\infty} U_{zns} \cos(n\theta) \exp(-jk_{ns}x + j\omega t) + U_{zmn}e^{j\omega t} \end{aligned} \tag{21}$$

The boundary and continuity conditions are the same as the x line force case except that everywhere the particular solution is added. The equations are again given in the form

$$Ay = B \tag{22}$$

Since the particular solution is known, several terms in the A matrix are known. These terms become the right-hand side forcing functions.

In presenting the response due to the transverse pressure load exerted by the piezoactuator, five different cases are presented for every circumferential mode n and frequency combination. For the first case, the actuator model developed is used [thus, the shell is

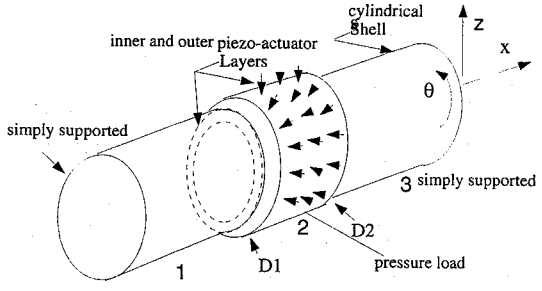

Fig. 9 Cylindrical shell with inside and outside surface-bonded ring piezoactuators; transverse pressure.

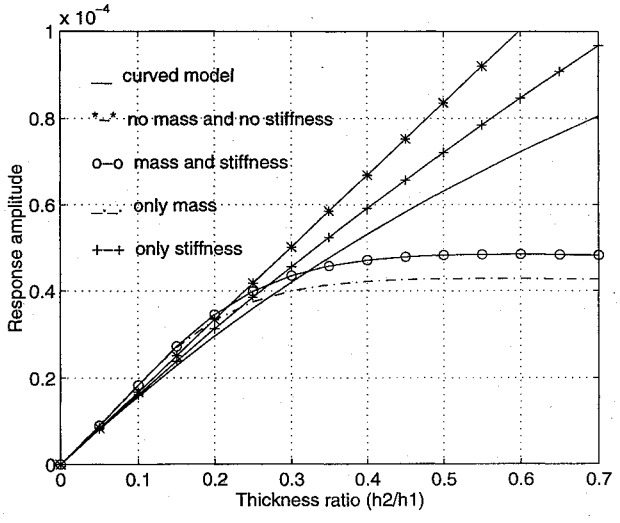

Fig. 10 Shell response as a function of thickness ratio; transverse pressure and (3, 3) mode resonance frequency of 394 Hz.

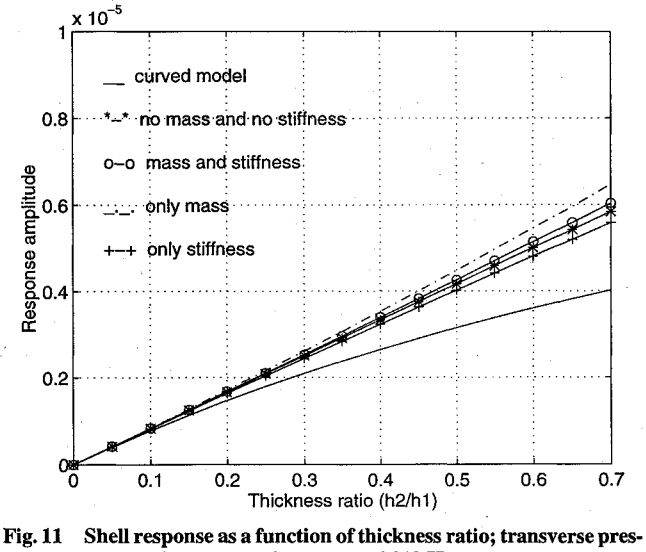

Fig. 11 Shell response as a function of thickness ratio; transverse pressure and n = 3 off-resonance frequency of 318 Hz.

homogenous with an applied pressure, Eq. (10) F_z]; the second involves the full shell/actuator system [in computing the wave numbers the actuator stiffness and density are used, and for equivalent force the right side of Eq. (3) is used]; the third case accounts only for the actuator stiffness (in computing the wave numbers for the composite region, the actuator density is set to zero); and the fourth case involves only the density of the system (in computing the wave numbers for the composite part the stiffness is set to zero). Thus, for the curved model case the pressure load expression is given by F_z in Eq. (10). For the other three cases, the force expression is given by right side of Eq. (3). The fifth and last case also involves the right side of Eq. (3) but with the actuator mass and stiffness set to zero. The pressure load is exerted as shown in Fig. 9.

The results investigated include a resonance and an off-resonance case for each of the circumferential modes $n = 1, 2, 3, 4, 15$, and 16. But only resonance and off-resonance cases for $n = 3$ and 4 and an off-resonance case for $n = 15$ are shown. This is to limit the length of the manuscript. However, all the investigated results are used in presenting the discussion.

Figures 10–14 show the response of the shell at $x = 2.25$ m for the five different cases mentioned as the actuator/shell thickness ratio is varied. Figures 10 and 11 are for $n = 3$, Figs. 12 and 13 for $n = 4$, and Fig. 14 for $n = 15$. Figures 12 and 13 for $n = 3$ and 4 correspond to a resonance and an off-resonance frequency. In general (from all cases investigated), from the composite response and those with either mass or stiffness and for off-resonance cases at lower n numbers, neither the mass nor the stiffness of the actuators seems to have a significant effect on the response. This may be seen by comparing with the case that has no actuator property but is forced by Eq. (3). The responses are very close even up to a thickness of 1.5 mm (shell thickness is 2 mm). This behavior is seen even for high n cases at low off-resonances (not shown) and resonances. This is not the case for higher order n at high frequencies. It may be that the longitudinal wave generated by the pressure in the z direction is resisted mainly by the shell and its supports so that the actuator properties do not contribute to the resistance. The reason for this behavior is not fully clear, but it appears that the expression given by right side of Eq. (3) is a good model for low off-resonance frequencies for all n. The model thus will predict the response with

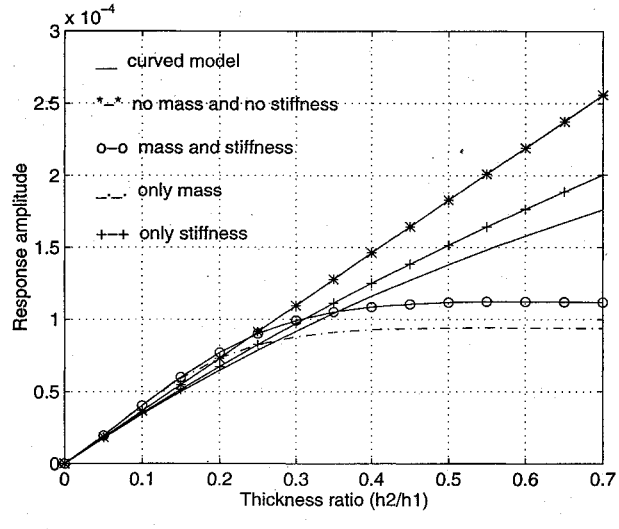

Fig. 12 Shell response as a function of thickness ratio; transverse pressure and (3, 4) mode resonance frequency of 271 Hz.

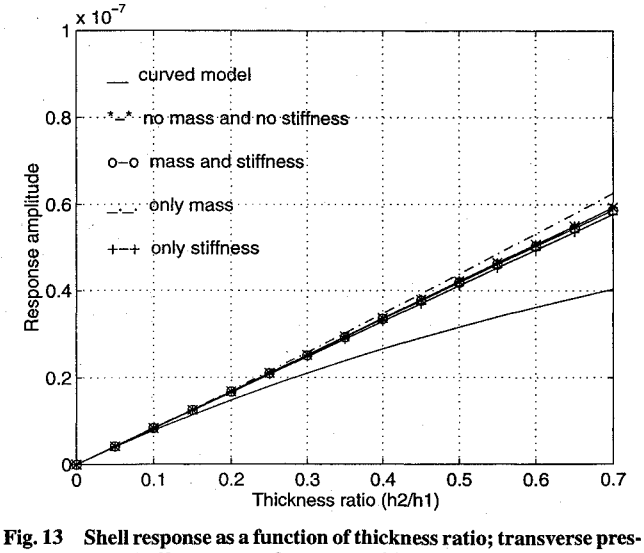

Fig. 13 Shell response as a function of thickness ratio; transverse pressure, and n = 4 off-resonance frequency of 398 Hz.

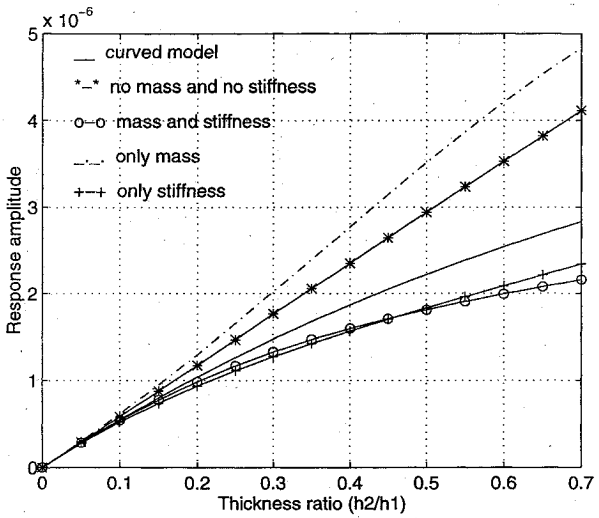

Fig. 14 Shell response as a function of thickness ratio; transverse pressure and n = 15 off-resonance frequency of 1250 Hz.

reasonable accuracy if the actuator parameters (size, location, etc.) are tailored to excite lower n modes of the shell.

The piezoactuator equivalent forces are derived using simple force balance equations and hence are related to one another. Thus, even though the exact behavior of the shell to the θ line force cannot be predicted using this configuration, it can be said with sufficient confidence that the derived model will predict the response at low n resonances and off-resonances. And for the shell size chosen the corresponding thickness ratio limits will be 0.25 and 0.5.

Conclusions

x Line Force

Some generalizations may be made from the cases studied earlier. The curved model performs reasonably well at off-resonances even up to half the shell thickness for low-circumferential modes. In contrast, at resonance frequencies the dynamic effects of the actuator take over much earlier. The model in most resonance cases for low n is valid at most up to 0.25 of the shell thickness. The mass of the actuator seems to be the dominant effect at resonances so that small-sized actuators promise to do better. The axial line force does not couple well into higher order circumferential modes. The response is low, and the model differs significantly from the other cases. However, as mentioned earlier, if the actuator dimensions and other control parameters are tailored for low-circumferential shell mode excitation, the current model will represent the response reasonably well.

Transverse Pressure

For the pressure load, the force expression in the composite shell Eq. (3) performs far better than the derived model expression. The reason at this point is unknown, but it appears that at off-resonances and at resonances the actuator mass or the density has small effect on the response. For off-resonance the effect is negligible even up to half the thickness of the actuator, whereas for resonances it is up to quarter thickness of the shell. Based on the pressure model, the θ line force expression may be obtained that is the line force expression in Eq. (2).

References

[1]Bailey, T., and Hubbard, J. E., "Distributed Piezoelectric-Polymer Active Vibration Control of a Cantilever Beam," *Journal of Guidance, Control, and Dynamics*, Vol. 8, No. 5, 1985, pp. 605–611.

[2]Baz, A., and Poh, S., "Optimum Vibration Control of Flexible Beams by Piezoelectric Ceramics," NASA CR-180209, 1987.

[3]Dimitriadis, E. K., Fuller, C. R., and Rogers, C. A., "Piezoelectric Actuators for Distributed Excitation of Thin Plates," *Journal of Vibration and Acoustics*, Vol. 113, 1991, pp. 100–107.

[4]Lee, C. K., "Piezoelectric Laminates for Torsional and Bending Modal Control: Theory and Experiment," Ph.D. Thesis, Cornell Univ., Ithaca, NY, 1987.

[5]Fuller, C. R., Snyder, S., Hansen, C., and Silcox, R., "Active Control of Interior Noise in Model Aircraft Fuselages Using Piezoceramic Actuators," AIAA Paper 90-3922, Oct. 1990.

[6]Lester, H. C., and Lefebvre, S., "Piezoelectric Actuator Models for Active Sound and Vibration Control of Cylinders," *Proceedings of Recent Advances in Active Noise and Vibration Control*, Blacksburg, VA, April 1991, pp. 3–26.

[7]Lester, H. C., and Silcox, R. J., "Active Control of Interior Noise in a Large Scale Cylinder Using Piezoceramic Actuators," International Technical Specialists Meeting, Rotorcraft Acoustics and Rotor Fluid Dynamics, American Helicopter Society, Valley Forge, PA, Oct. 1991.

[8]Silcox, R. J., Lefebvre, S., Metcalf, V. L., Beyer, T. B., and Fuller, C. R., "Evaluation of Piezoceramic Actuators for Control of Aircraft Interior Noise," DGLR/AIAA 14th Aeroacoustics Conference, Paper 92-02-91, Aachen, Germany, May 1992.

[9]Masters, A. A., Kim, S. J., and Jones, J. D., "Experimental Investigation into Active Control of Compressor Noise Radiation Using Piezoelectric Actuators," *Inter-Noise 92*, Toronto, ON, Canada, July 1992, pp. 395–400.

[10]Sonti, V. R., and Jones, J. D., "Curved Piezo-Actuator Model for Active Vibration Control of Cylindrical Shells," *AIAA Journal* (submitted for publication).

[11]Soedel, W., *Vibrations of Plates and Shells*, Marcel Dekker, New York, 1981.

[12]Fuller, C. R., "The Effects of Wall Discontinuities on the Propagation of Flexural Waves in Cylindrical Shells," *Journal of Sound and Vibration*, Vol. 75, No. 2, 1981, pp. 207–228.

[13]Leissa, A. W., "Vibrations of Shells," NASA SP-288, 1973.

[14]Sonti, V. R., "Analysis of Flat and Curved Piezo-Actuators for Vibration Control of Cylindrical Shells," Ph.D. Thesis, School of Mechanical Engineering, Purdue Univ., West Lafayette, IN, 1994.